SUPPLEMENTARY RESULTS

Supplementary Tables

Supplementary Table 1 | S1P receptor activation by S1P, *trans*-PhotoS1P and *cis*-PhotoS1P

Compound	$S1P_1$	$S1P_2$	$S1P_3$	$S1P_4$	$S1P_5$
	E_{max}, EC_{50}	E_{max}, EC_{50}	E_{max}, EC_{50}	E_{max}, EC_{50}	E_{max}, EC_{50}
S1P	100%, 18.4	100%, 92.7	100%, 10.4	100%, 24.4	100%, 82.1
***trans*-PhotoS1P**	60%, 12.7	10%, 352	74%, 81.0	-	93%, 60.0
***cis*-PhotoS1P**	60%, 45.8	40%, 247	29%, 91.4	51%, 234	98%, 88.3

Intracellular Ca^{2+} mobilization in response to S1P, *trans*-**PhotoS1P** and *cis*-**PhotoS1P** was measured in HTC4 cells expressing $S1P_{1-5}$. The responses are reported in terms E_{max} (% of S1P maximal response) and EC_{50} (nM).

Supplementary Table 2 | Target design for gene disruption using CRISPR/Cas9

Gene	Target	PAM	Plasmid	Cells
Sgpl1	cctctaacttccgtagtccg	ggg	pX330	McA-RH7777
Sgpp1	gactgctgcggtgcaccgaa	cgg	pX330	McA-RH7777
Sgpp2	ccaatcttctggacaaataa	ggg	pX330	McA-RH7777
Hprt1	cttttatgtcccccgttgac	tgg	pUC-U6-sg	McA-RH7777
SPHK1	ctggtgctgctgaacccgcg	cgg	pX330	HeLa MZ
SPHK2	tgagtgggatggcatcgtca	cgg	pX330	HeLa MZ
HPRT1	gtagccctctgtgtgctcaa	ggg	pUC-U6-sg	HeLa MZ

Supplementary Figures

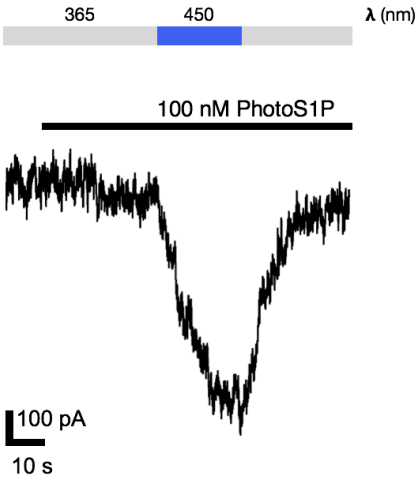

Supplementary Figure 1 | Optical Control of S1P1-GIRK coupling. A representative single current trace of **PhotoS1P** evaluated using whole-cell patch clamp recording in HEK293T cells transiently expressing $S1P_1$ receptors and GIRK channels. Application of **PhotoS1P** (100 nM) in *cis* state at 365 nm does not induce measurable currents. Activation at 450 nm light affords inward current which can be reversed at 365 nm light. This experiment was repeated 3 times with similar results.

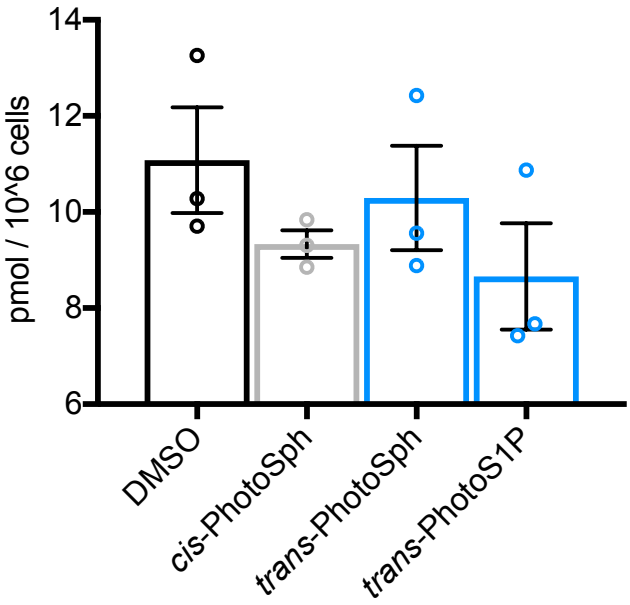

Supplementary Figure 2 | Photoswitchable Lipids do not alter level of endogenous lipids in WT HeLa MZ cells. Lipidomic quantification of C18 Sphingosine in HeLa MZ cells after treatment with DMSO, **PhotoSph** or **PhotoS1P** for 15 min. N = 3 biologically independent experiments. Error bars represent SEM.

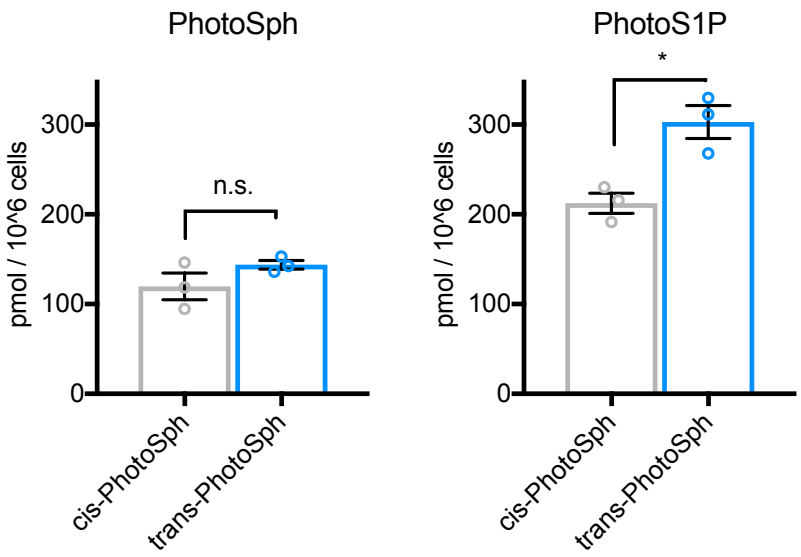

Supplementary Figure 3 | PhotoSph metabolism in WT RH7777 cells. Lipidomic quantification of **PhotoSph** and **PhotoS1P** in WT RH7777 cells after treatment with **PhotoSph** for 15 min (*p = 0.0135; n.s. = 0.2003; two-tailed student's t-test, N = 3 biologically independent experiments). Error bars represent SEM.

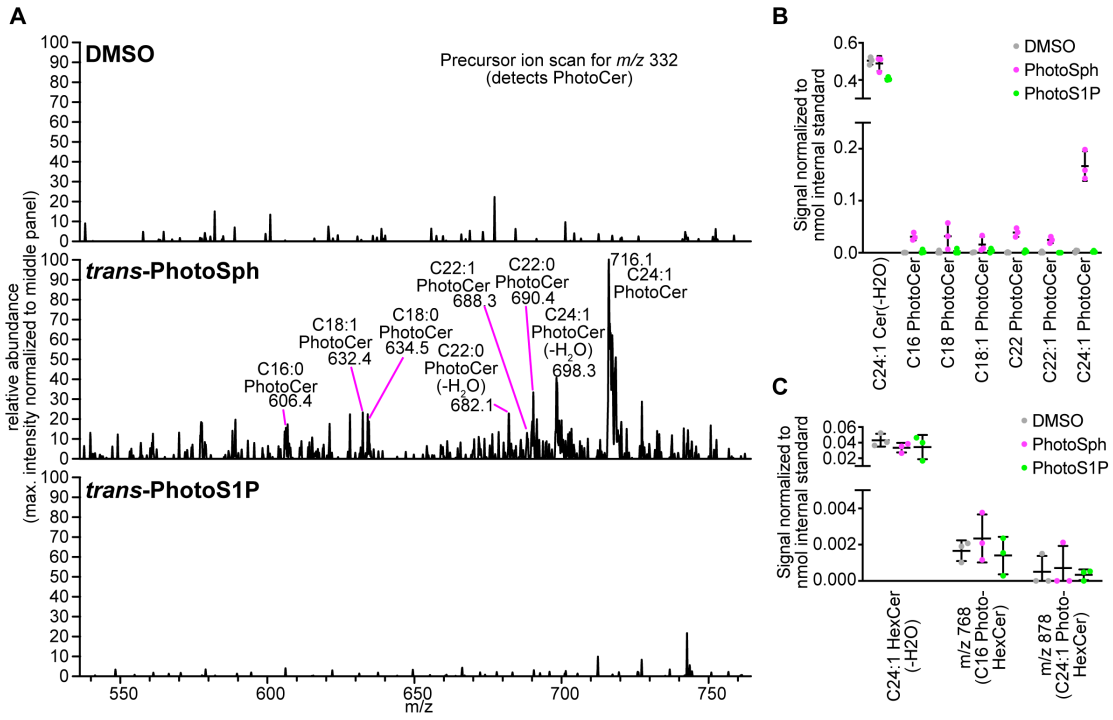

Supplementary Figure 4 | PhotoSph is converted into ceramides. (A) Lipids generating fragments of *m/z* 332 (**PhotoSph** with loss of two water molecules) were analyzed, using extracts from DMSO-, *trans*-**PhotoSph**-, or *trans*-**PhotoS1P**-treated cells (15 minutes treatment). Various ceramide species containing the azobenzene photoswitch (PhotoCer) were detected in *trans*-**PhotoSph**-treated cells, while being undetectable in DMSO- or *trans*-PhotoS1P-treated cells. Data is representative of three independent analyses with similar results. (B) Signal intensities of various PhotoCer species in **PhotoSph**-treated cells were in a range comparable to endogenous ceramide species. (C) Hexosylceramide (HexCer) species containing the azobenzene photoswitch (PhotoHexCer) were undetectable during the same analysis. Signal intensities of the indicated *m/z* values are shown, which would have corresponded to the PhotoHexCer species in parentheses, if present. (B,C) Error bars are standard deviations (n=3 biologically independent samples).

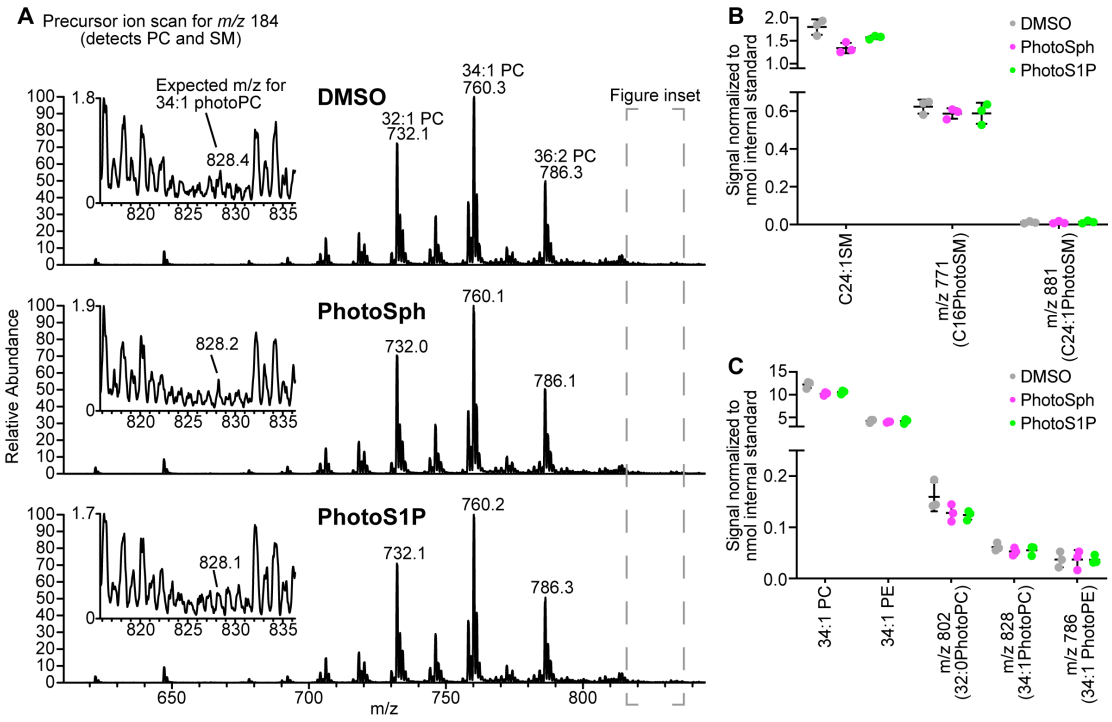

Supplementary Figure 5 | PhotoSph conversion into sphingomyelin and glycerophospholipids is undetectable. (A) Sphingomyelin (SM) and phosphatidylcholine (PC) were specifically analyzed by detecting lipids generating fragments of *m/z* 184 (phosphocholine), using extracts from DMSO-, *trans*-**PhotoSph**-, or *trans*-**PhotoS1P**-treated cells (15 minutes treatment). Signals corresponding to lipids bearing the azobenzene photoswitch did not exceed noise levels (example in figure inset). Data is representative of three independent analyses with similar results. (B,C) Signal intensities of the indicated *m/z* values are shown, which would have corresponded to the lipid species in parentheses, if present. Signals of abundant endogenous lipids are shown for comparison. The analysis of phosphatidylethanolamine (PE) was performed by detecting lipids that generate fragments having a neutral loss of *m/z* 141. The mass spectra are not depicted here and only quantification results are displayed. (B,C) Error bars are standard deviations (n=3 biologically independent samples).

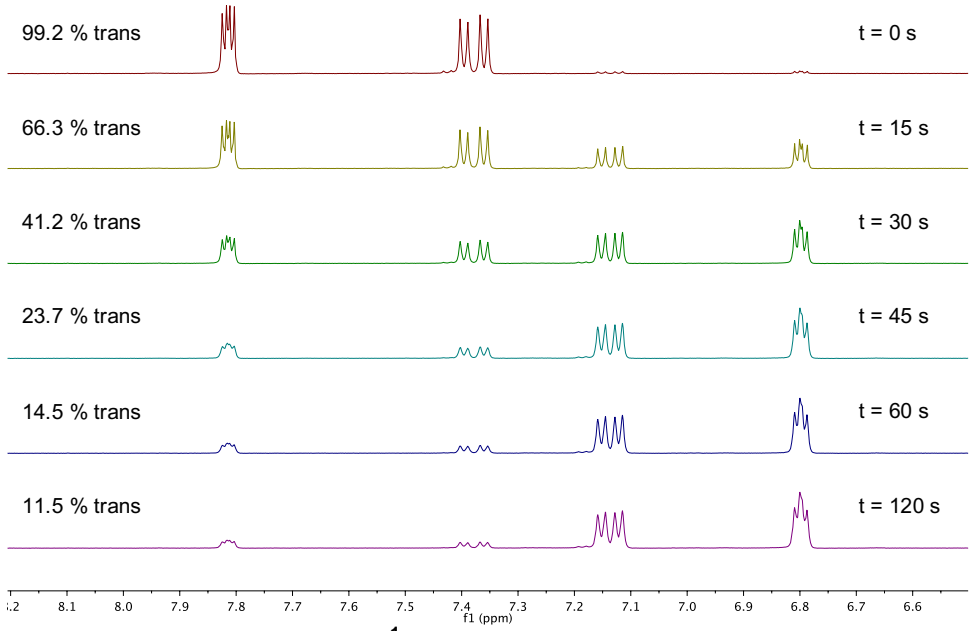

Supplementary Figure 6 | ^{1}H NMR of PhotoS1P after irradiation at 365 nm. **PhotoS1P** was dissolved in MeOD/ND_4OD and irradiated for varying durations at 365 nm to determine the photostationary states. In the dark-adapted state 99.2 % of **PhotoS1P** are *trans* while approx. 90% are *cis* after 2 minutes irradiation. Single Experiment.

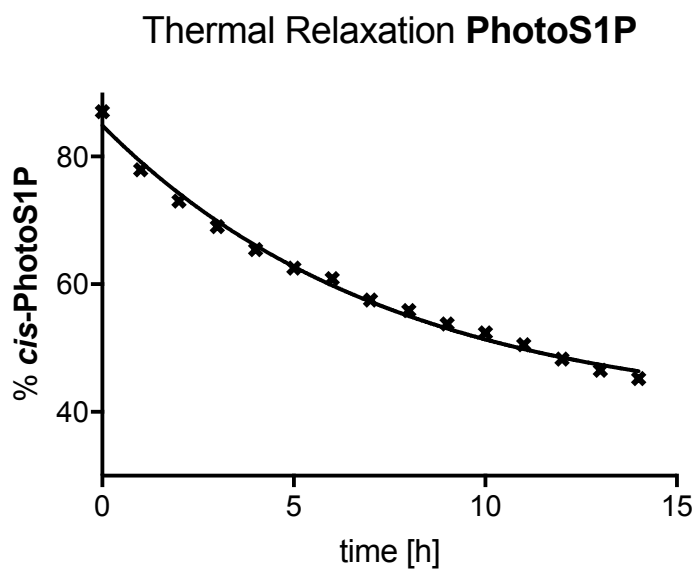

Supplementary Figure 7 | Thermal Relaxation of PhotoS1P as determined by ^{1}H NMR. PhotoS1P was dissolved in MeOD/ND_4OD and irradiated for 2 minutes at 365 nm. A proton NMR was recorded every hour for 14 h at 37 ºC and the % of *cis*-**PhotoS1P** were plotted as a function of time. The thermal relaxation half life was 18.4 h. Single Experiment.

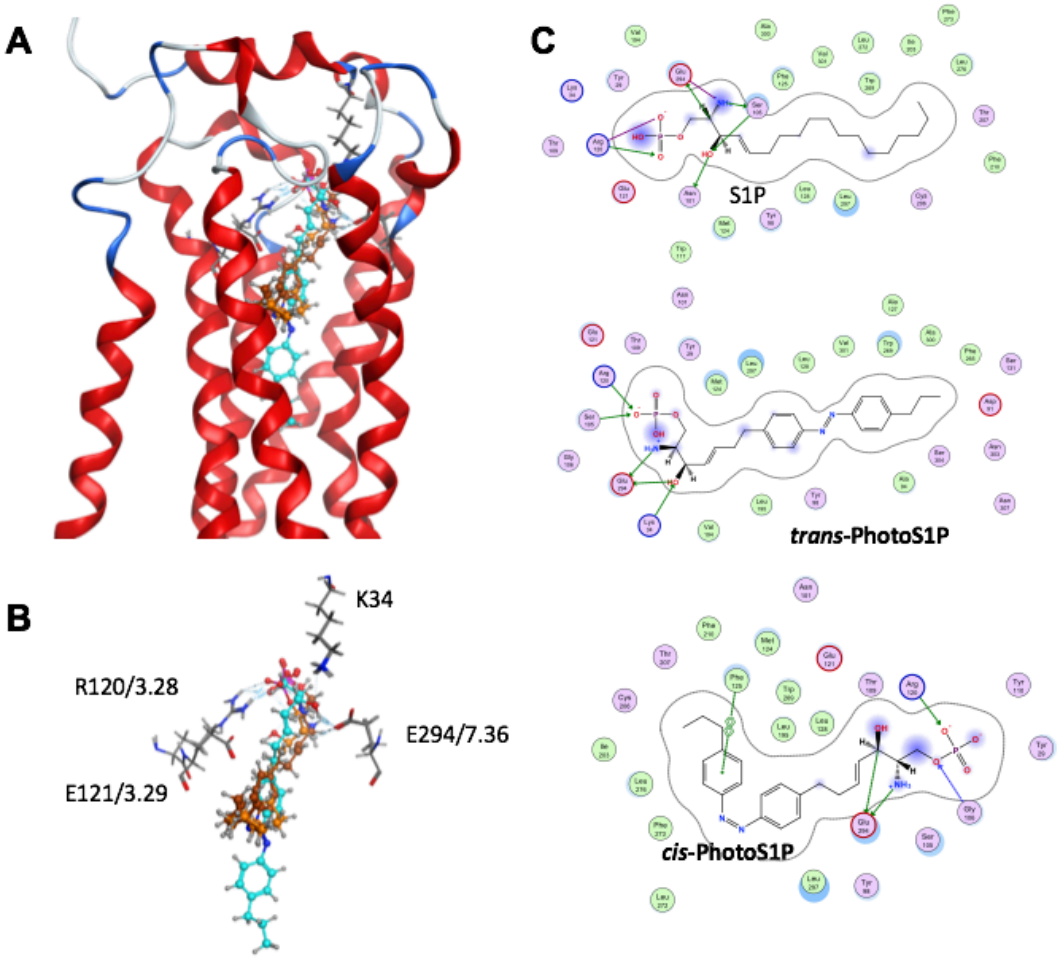

Supplementary Figure 8 | Model $S1P_1$ receptor in complex with S1P and PhotoS1P. (A) $S1P_1$ receptor model in complex with S1P (orange), ***trans*-PhotoS1P** (cyan), and ***cis*-PhotoS1P** (brown). (B) Same view as (A) but only subset of engaging residues shown. (C) S1P, ***trans*-PhotoS1P**, and ***cis*-PhotoS1P** with proximate residues in binding pocket and engaging residues highlighted using green to indicate sidechain interactions and blue to indicate backbone interactions. Arrows point toward the hydrogen bond acceptor in hydrogen bonding interactions.

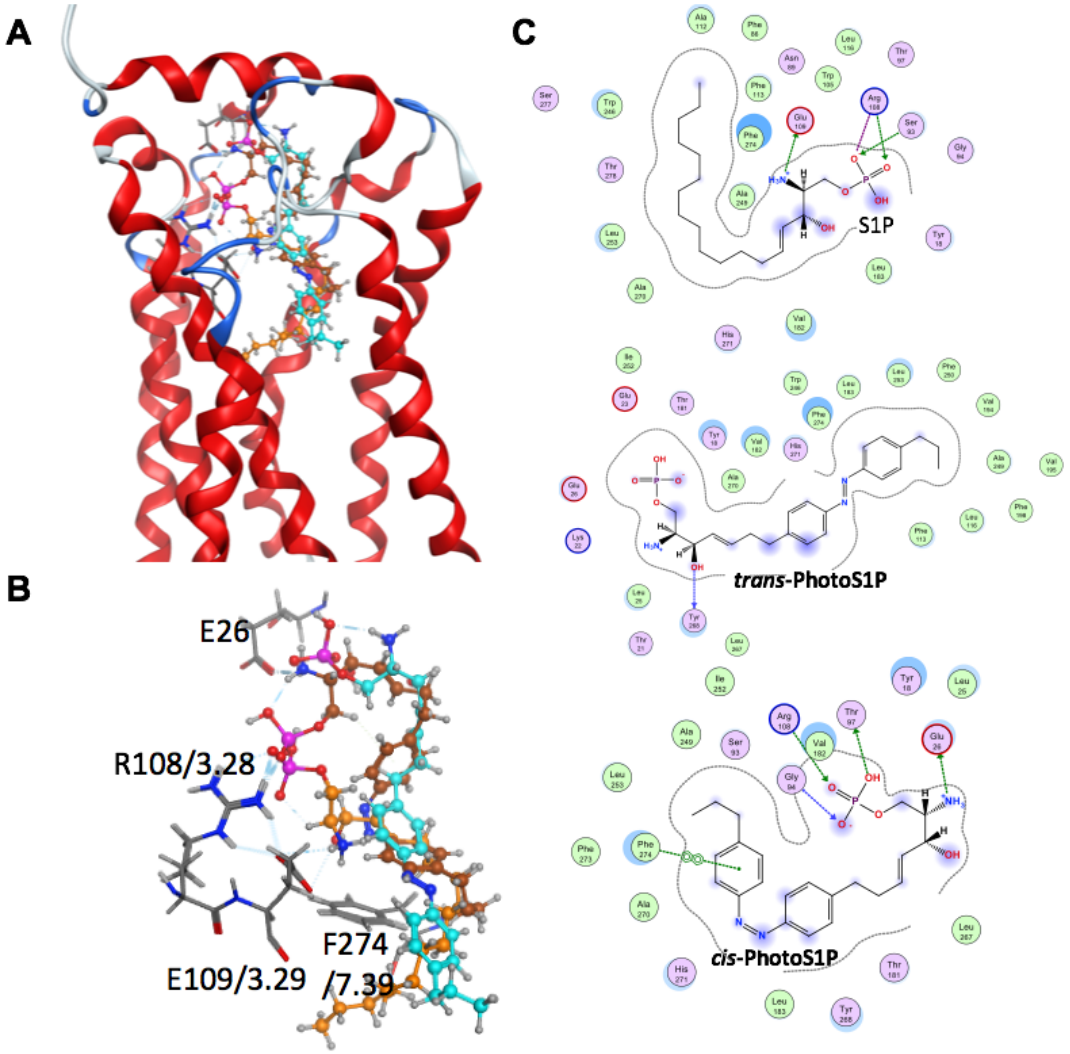

Supplementary Figure 9 | Model $S1P_2$ receptor in complex with S1P and PhotoS1P. (A) $S1P_2$ receptor model in complex with S1P (orange), ***trans*-PhotoS1P** (cyan), and ***cis*-PhotoS1P** (brown). (B) Same view as (A) but only subset of engaging residues shown. (C) S1P, ***trans*-PhotoS1P**, and ***cis*-PhotoS1P** with proximate residues in binding pocket and engaging residues highlighted using green to indicate sidechain interactions and blue to indicate backbone interactions. Arrows point toward the hydrogen bond acceptor in hydrogen bonding interactions.

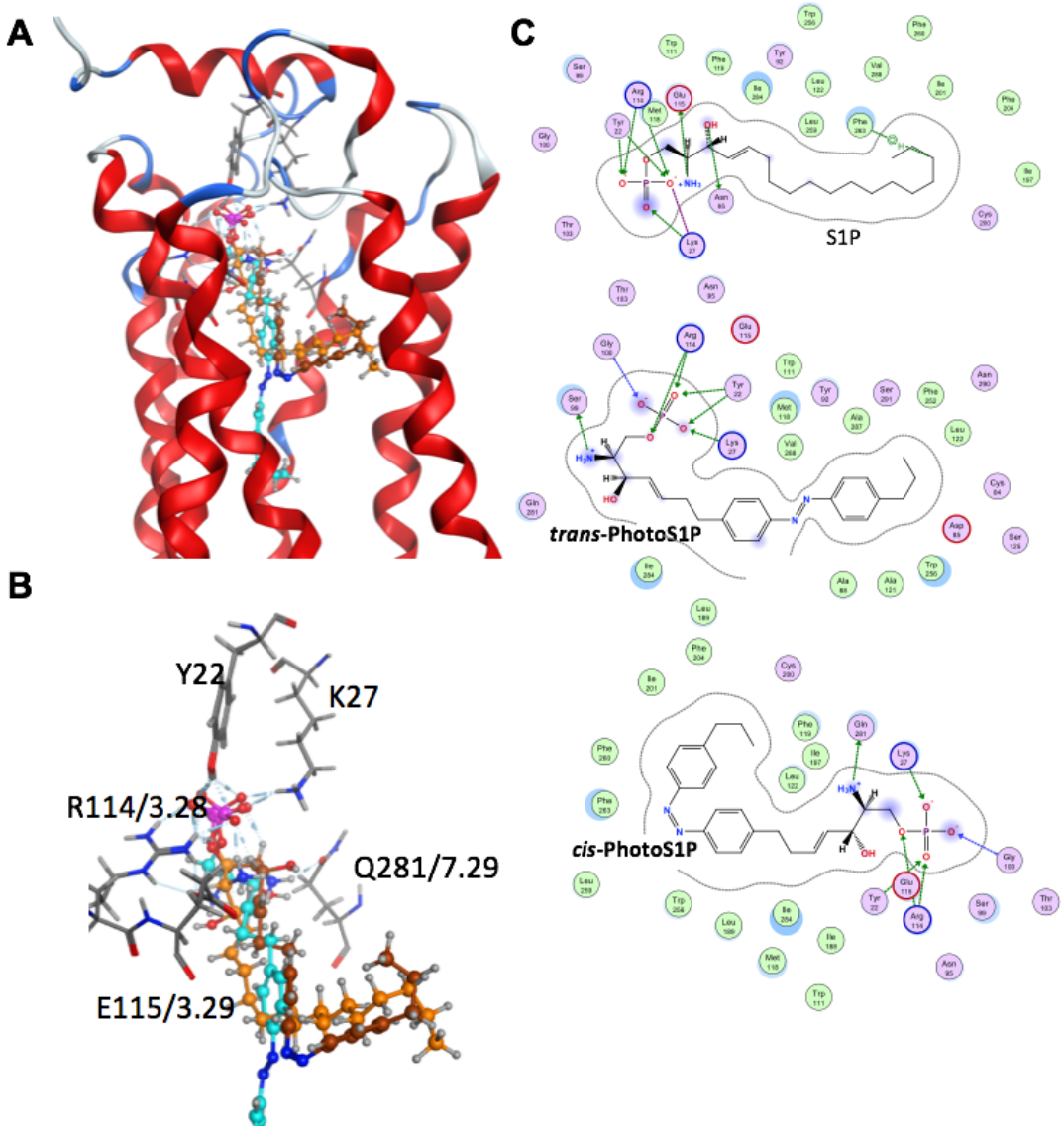

Supplementary Figure 10 | Model $S1P_3$ receptor in complex with S1P and PhotoS1P. (A) $S1P_3$ receptor model in complex with S1P (orange), ***trans*-PhotoS1P** (cyan), and ***cis*-PhotoS1P** (brown). (B) Same view as (A) but only subset of engaging residues shown. (C) S1P, ***trans*-PhotoS1P**, and ***cis*-PhotoS1P** with proximate residues in binding pocket and engaging residues highlighted using green to indicate sidechain interactions and blue to indicate backbone interactions. Arrows point toward the hydrogen bond acceptor in hydrogen bonding interactions.

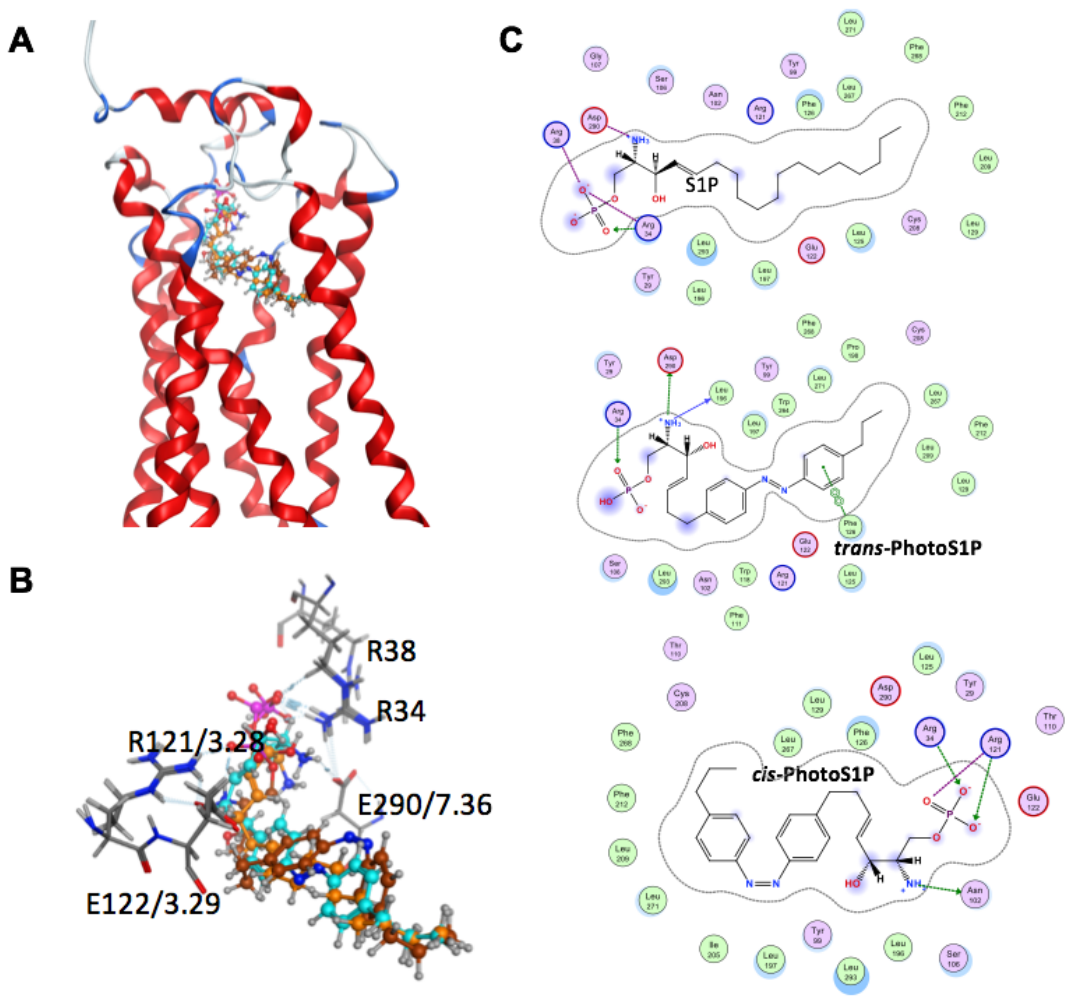

Supplementary Figure 11 | Model $S1P_4$ receptor in complex with S1P and PhotoS1P. (A) $S1P_4$ receptor model in complex with S1P (orange), ***trans*-PhotoS1P** (cyan), and ***cis*-PhotoS1P** (brown). (B) Same view as (A) but only subset of engaging residues shown. (C) S1P, ***trans*-PhotoS1P**, and ***cis*-PhotoS1P** with proximate residues in binding pocket and engaging residues highlighted using green to indicate sidechain interactions and blue to indicate backbone interactions. Arrows point toward the hydrogen bond acceptor in hydrogen bonding interactions.

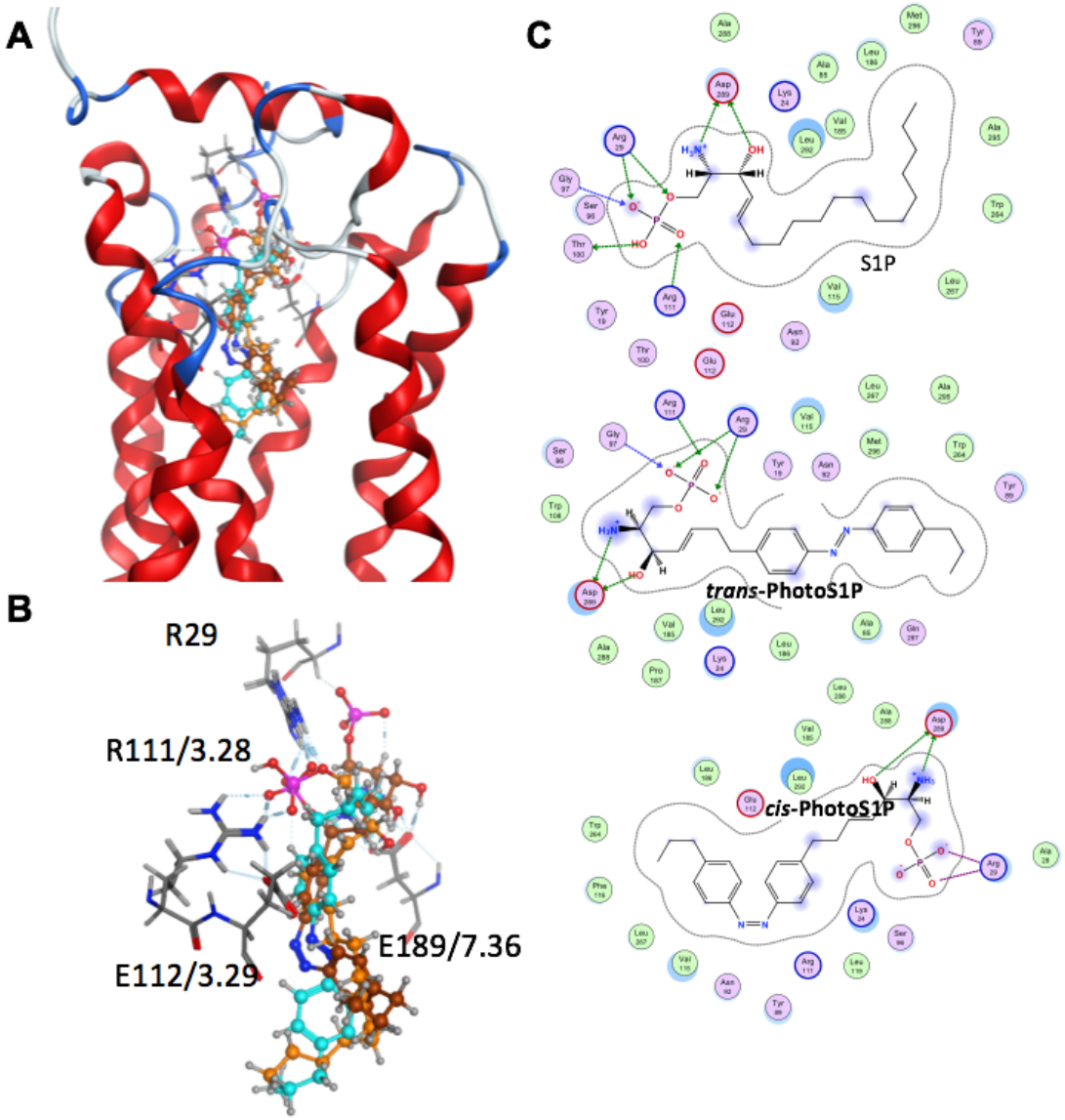

Supplementary Figure 12 | Model $S1P_5$ receptor in complex with S1P and PhotoS1P. (A) $S1P_5$ receptor model in complex with S1P (orange), ***trans*-PhotoS1P** (cyan), and ***cis*-PhotoS1P** (brown). (B) Same view as (A) but only subset of engaging residues shown. (C) S1P, ***trans*-PhotoS1P**, and ***cis*-PhotoS1P** with proximate residues in binding pocket and engaging residues highlighted using green to indicate sidechain interactions and blue to indicate backbone interactions. Arrows point toward the hydrogen bond acceptor in hydrogen bonding interactions.